

Non-perturbative computation of double inclusive gluon production in the Glasma

T. Lappi

*Physics Dept., P.O. Box 35, 40014, University of Jyväskylä and
Helsinki Institute of Physics, P.O. Box 64, 00014 University of Helsinki, Finland
Email: tuomas.lappi@jyu.fi*

S. Srednyak

*Physics Dept., SUNY Stony Brook, Stony Brook, NY 11790 and
Physics Dept., Bldg. 510A, Brookhaven National Laboratory, Upton, NY 11973, USA
Email: stas_srednyak@yahoo.com*

R. Venugopalan

*Physics Dept., Bldg. 510A, Brookhaven National Laboratory, Upton, NY 11973, USA
Email: rajuv@mac.com*

ABSTRACT: The near-side ridge observed in A+A collisions at RHIC has been described as arising from the radial flow of Glasma flux tubes formed at very early times in the collisions. We investigate the viability of this scenario by performing a non-perturbative numerical computation of double inclusive gluon production in the Glasma. Our results support the conjecture that the range of transverse color screening of correlations determining the size of the flux tubes is a semi-hard scale, albeit with non-trivial structure. We discuss our results in the context of ridge correlations in the RHIC heavy ion experiments.

Contents

1. Introduction	1
2. Perturbative results for multi-particle production	5
3. Non-perturbative computation	7
3.1 Numerical approach	8
3.2 Parameters in the computation	10
3.3 Relating $g^2\mu_A$ and Q_s on the lattice	10
4. Results	13
4.1 Single inclusive spectrum	13
4.2 Double inclusive spectrum	14
4.3 Determining κ_2	15
5. Discussion and physical interpretation of results	17
6. Summary	20
7. Acknowledgments	20
A. Lattice formulation	20

1. Introduction

At very high energies, the collision of two nuclei can be conveniently described as the collision of two Color Glass Condensates (CGCs) [1, 2, 3]. In this description, the wavefunctions of the nuclei are comprised of high occupation number classical gluon fields at small x coupled to static light cone color sources at large x . The separation between fields and sources evolves with energy; one obtains evolution equations for multi-parton correlations in the nuclear wavefunctions called JIMWLK renormalization group equations [2]. After the collision, the coherence of the nuclear wavefunction is lost; large x sources are no longer static and become sources for multi-particle production in the forward light cone [4]. For early times $\tau \sim 1/Q_s$, where Q_s is the saturation scale, the non-equilibrium produced matter with high occupation number of order $1/\alpha_s$ has remarkable properties [5, 6] and is termed the Glasma [7]. For reviews, see Ref. [8].

Recently, high energy factorization theorems were derived for inclusive multi-gluon production in a rapidity interval $\Delta y \lesssim 1/\alpha_s$ [9, 10] in A+A collisions. The result can be expressed very compactly as [10]

$$\left\langle \frac{d^n N_n}{d^3 \mathbf{p}_1 \cdots d^3 \mathbf{p}_n} \right\rangle_{\text{LLog}} = \int [D\rho_1][D\rho_2] Z_y[\rho_1] Z_y[\rho_2] \left. \frac{dN}{d^3 \mathbf{p}_1} \right|_{\text{LO}} \cdots \left. \frac{dN}{d^3 \mathbf{p}_n} \right|_{\text{LO}} . \quad (1.1)$$

The Z 's are gauge invariant weight functionals that describe the distribution of color sources at the rapidity of interest. They are obtained in full generality by evolving the JIMWLK equations from an initial rapidity close to the beam rapidity. In the large N_c limit, the weight functionals Z can instead be obtained from the simpler mean field Balitsky–Kovchegov (BK) [11] equation. In this case, they can be represented as non-local Gaussian distributions in the sources [12]. For large nuclei, without significant small x evolution, one recovers the local Gaussian distributions of the McLerran-Venugopalan (MV) model [1]. We emphasize that the validity of eq. (1.1) is restricted to the kinematics where all the produced particles are measured within a rapidity interval $\lesssim 1/\alpha_s$ from each other, so that we can evaluate Z at this same rapidity $y_1 \approx \cdots \approx y_n \approx y$. The generalization to larger rapidity separations is non-trivial because one needs to account for the gluon radiation in the region between the tagged gluons. A formalism describing arbitrarily long range rapidity separations has been developed recently [13]. For simplicity, we shall not consider it further here.

The leading order single particle distributions in eq. (1.1) are given by

$$E_{\mathbf{p}} \left. \frac{dN}{d^3 \mathbf{p}} \right|_{\text{LO}} [\rho_1, \rho_2] = \frac{1}{16\pi^3} \lim_{x_0 \rightarrow +\infty} \int d^3 \mathbf{x} d^3 \mathbf{y} e^{ip \cdot (x-y)} (\partial_x^0 - iE_{\mathbf{p}})(\partial_y^0 + iE_{\mathbf{p}}) \\ \times \sum_{\lambda} \epsilon_{\lambda}^{\mu}(\mathbf{p}) \epsilon_{\lambda}^{\nu}(\mathbf{p}) A_{\mu}^{a,\text{cl.}}[\rho_1, \rho_2](x) A_{\nu}^{a,\text{cl.}}[\rho_1, \rho_2](y) . \quad (1.2)$$

For each configuration of sources ρ_1 and ρ_2 respectively, of each of the nuclei, one can solve classical Yang–Mills equations to compute the gauge fields $A_{\mu}^{\text{cl.}}[\rho_1, \rho_2]$ in the forward light cone [14, 15, 16, 17, 18]. When our expression for the corresponding single inclusive distribution is substituted in eq. (1.1), and the distributions are averaged over with the distributions Z , one has determined from first principles (to all orders in perturbation theory and to leading logarithmic accuracy¹ in x), the n-gluon inclusive distribution in high energy A+A collisions at proper times $\tau \sim 1/Q_s$. As noted previously, eq. (1.1) is valid only for $\Delta Y \lesssim 1/\alpha_s \sim 3 - 5$ units of rapidity in A+A collisions at RHIC and the LHC respectively.

In the nuclei, before the collision, the typical range of color correlations is of the order of the inverse saturation scale Q_s^{-1} , where $Q_s^{-1} < \Lambda_{\text{QCD}}^{-1}$. The saturation scale at a given transverse position in the nucleus depends on the two dimensional transverse projection of the nuclear matter distribution. In eq. (1.1), it appears in the initial conditions for the Z functionals; the energy evolution of the saturation scale is determined by the JIMWLK

¹Note that what we mean by leading log of x here means resumming the leading dependence in rapidity between the observed gluons and the projectiles; not between the different produced gluons.

renormalization group equations. Because the saturation scales in the two nuclei are the only scales in the problem (besides nuclear radii), their properties determine the energy and centrality dependence of the inclusive observables.

The expression in eq. (1.1) is remarkable because it suggests that in a single event—corresponding to a particular configuration of color sources—the leading contribution is from n tagged gluons that are produced independently. The coherence in n -gluon emission is generated by averaging over color sources that vary from event to event. Because the range of color correlations in the transverse plane is of order $1/Q_s$, the high energy factorization formalism suggests an intuitive picture of correlated multiparticle production arising from event by event fluctuations in particle production from $\sim R_A^2/1/Q_s^2 = R_A^2 Q_s^2$ color flux tubes of size $1/Q_s$.

The color flux tubes, called Glasma flux tubes, are approximately boost invariant in rapidity because of the underlying boost invariance of the classical fields². Besides providing the underlying geometrical structure for long range rapidity correlations, the Glasma flux tubes also carry topological charge [6], which may result in observable metastable CP-violating domains [19]. While eqs. (1.1) and (1.2) describe particle production from the Glasma flux tubes, they do not describe the subsequent final state interactions of the produced gluons which become important for times $\tau \gg 1/Q_s$.

If, as widely believed, the produced matter thermalizes by final state interactions, these will not significantly alter long range rapidity correlations because the effects of fragmentation, hadronization or resonance decays are typically restricted to $\Delta y \approx 1 \ll 1/\alpha_s$. However, radial flow will have a significant effect on the observed angular correlations. This is because particles produced isotropically in a given flux tube will be correlated by the radial outward hydrodynamic flow of the flux tubes. Ideas on the angular collimation of particle distributions by flow were discussed previously in the literature [20, 21]. When combined with the long range rapidity correlations provided by the Glasma flux tubes, they provide a natural explanation [22, 23] of “ridge” like structures [24, 25] seen in the nearside spectrum of two particle correlated hadron pairs in A+A collisions. A similar structure is seen in three hadron correlations as well [26].

These structures were first seen in near side events with prominent jet like structures, where the spectrum of associated particles is observed to be collimated in the azimuthal separation $\Delta\varphi$ relative to the jet and shows a nearly constant amplitude in the strength of the pseudo-rapidity correlation $\Delta\eta$ up to $\Delta\eta \sim 1.5$ [24]. The name “ridge” follows from the visual appearance of these structures as an extended mountain ridge in the $\Delta\eta$ - $\Delta\varphi$ plane associated with a narrow jet peak. This collimated correlation persists up to $\Delta\eta \sim 4$ [27]. An important feature of ridge correlations is that the above described structure is seen in two particle correlations without a jet trigger and persists without significant modification for the triggered events [28]. These events include all hadrons with momenta $p_T \geq 150$ MeV. In such events, a sharp rise in the amplitude of the ridge is seen [28, 29] in going from peripheral to central collisions. A number of theoretical

²For rapidity separations $\gtrsim 1/\alpha_s$, one expects significant violations of boost invariance from quantum corrections [13].

models have been put forth to explain these ridge correlations [21, 30]. For a recent critical evaluation of these models, we refer the reader to Ref. [31].

In this paper, our primary purpose is to discuss how the Glasma flux tube picture arises *ab initio* from solving eqs. (1.1) and (1.2). In Ref. [22], it was argued that the two particle correlation function

$$C_2(\mathbf{p}, \mathbf{q}) \equiv \left\langle \frac{d^2 N_2}{dy_p d^2 \mathbf{p}_T dy_q d^2 \mathbf{q}_T} \right\rangle - \left\langle \frac{dN}{dy_p d^2 \mathbf{p}_T} \right\rangle \left\langle \frac{dN}{dy_q d^2 \mathbf{q}_T} \right\rangle, \quad (1.3)$$

in the Glasma flux tube picture took on the simple geometrical form

$$\frac{C_2(\mathbf{p}, \mathbf{q})}{\left\langle \frac{dN}{dy_p d^2 \mathbf{p}_T} \right\rangle \left\langle \frac{dN}{dy_q d^2 \mathbf{q}_T} \right\rangle} = \kappa_2 \frac{1}{S_\perp Q_s^2}, \quad (1.4)$$

where the right hand side of this relation is simply a non-perturbative constant κ_2 multiplied by the ratio of the transverse area of the flux tube to the transverse overlap area of the nuclei. This nice geometrical identity however is a conjecture based on a perturbative computation whose regime of validity is the kinematic region $p_T, q_T \gg Q_s$, where one expects additional contributions, besides those arising from strong sources, to contribute significantly. Similar arguments, based on perturbative computations were used to generalize the result in eq. (1.4) to 3-particle correlations [32] and subsequently, even n -particle correlations [33]. In the latter paper, it was shown that the general structure of n -gluon emissions is a negative binomial distribution.

Because the geometrical structure of the correlations is so striking and with manifest consequences, it is important to establish that it has a validity beyond perturbation theory. The perturbative expressions extended to lower momenta are strongly infrared divergent so it is not obvious whether they are regulated in that regime by the confinement scale of the order of Λ_{QCD} or instead a semi-hard scale of order Q_s^{-1} arising from the weak coupling albeit non-perturbative dynamics of the Glasma fields. We will tackle the problem head-on in this paper and investigate the form of eq. (1.3) in this paper. We will do so by solving the Yang–Mills equations in eq. (1.2) in full generality numerically on a space-time lattice. Our non-perturbative results from the lattice simulations are valid³ in the entire kinematic domain of transverse momenta—from the smallest infrared scale given by the lattice size to the largest ultraviolet scale given by the lattice spacing. In physical units, these correspond to the inverse nuclear size and large momenta ($p_T, q_T \gg Q_s$).

One can of course, on dimensional grounds, always express the r.h.s of eq. (1.4) as shown. However, κ_2 in general can depend on the dimensionless ratios Q_s/p_T , Q_s/q_T , the relative azimuthal angle $\Delta\varphi$ between the two gluons, and the dimensionless combinations $Q_s R_A$ and m/Q_s , where m is an infrared scale of order Λ_{QCD} and R_A is the nuclear radius. We will examine the dependence of κ_2 on these parameters carefully and discuss what they tell us about the structure of correlations. We find that the Glasma flux tube picture is valid; however, while the size of transverse correlations is still a semi-hard scale, it is not

³We emphasize however that at very large momenta there will be additional contributions to the distributions beyond the purely classical one discussed here.

simply Q_s and does display some sensitivity to infrared physics. Our results are important for quantitative explanations of the ridge as resulting from Glasma flux tubes. In the semi-quantitative computation of Ref. [23], κ_2 was implicitly taken to be a free parameter and fit to the data—we will compare our result to this value. We will also compare our result to the value obtained by comparing the Glasma multiplicity distribution [33] to PHENIX data on multiplicity distributions at RHIC [34].

In section 2, we will review perturbative computations of multi-particle production in the Glasma. The non-perturbative computation will be discussed in Section 3. We will briefly outline the numerical approach, clearly stating the lattice parameters, their relation to physical parameters, and the approach to the continuum limit in the transverse and longitudinal co-ordinates. We will then systematically study the dependence of our results on the saturation scale, the nuclear size and the infrared cutoff m . In section 4, we will discuss the physical implications of our results and further refinements for quantitative comparison with experiment. We will end with a brief summary of our key results. Some details of the numerical computation are discussed in an appendix.

2. Perturbative results for multi-particle production

The perturbative computation of two, three and n -gluon correlations in the Glasma have been discussed elsewhere [22, 32, 33]. For completeness, we will briefly review the results here. The correlated two particle inclusive distribution can be expressed as

$$C(\mathbf{p}, \mathbf{q}) = \frac{1}{4(2\pi)^6} \sum_{a, a'; \lambda, \lambda'} \left\langle |\mathcal{M}_{\lambda\lambda'}^{aa'}(\mathbf{p}, \mathbf{q})|^2 \right\rangle - \langle |\mathcal{M}_\lambda^a(\mathbf{p})|^2 \rangle \langle |\mathcal{M}_{\lambda'}^{a'}(\mathbf{q})|^2 \rangle, \quad (2.1)$$

where the classical contribution to the amplitude for the production of a pair of gluons with momenta \mathbf{p} and \mathbf{q} is

$$\begin{aligned} \mathcal{M}_{\lambda\lambda'}^{aa'}(\mathbf{p}, \mathbf{q}) &= \epsilon_\mu^\lambda(\mathbf{p}) \epsilon_\nu^{\lambda'}(\mathbf{q}) p^2 q^2 A^{\mu, a}(\mathbf{p}) A^{\nu, a'}(\mathbf{q}), \\ \mathcal{M}_\lambda^a(\mathbf{p}) &= \epsilon_\mu^\lambda(\mathbf{p}) p^2 A^{\mu, a}(\mathbf{p}). \end{aligned} \quad (2.2)$$

Here the ϵ 's are the polarization vectors of the gluons and a, a' are the color indices of the gauge fields. The average $\langle \dots \rangle$ in eq. (2.1) is an average over the color configurations of the two nuclei; this average will be discussed further shortly.

The gauge fields have a very non-trivial, non-linear dependence on the sources ρ_1 and ρ_2 , which evolves as a function of the proper time τ . As mentioned previously, they can be determined by numerically solving Yang-Mills equations for $\tau \geq 0$ with initial conditions at $\tau = 0$ given by the gauge fields of each of the nuclei before the collision [14, 15, 17]. We will discuss these numerical solutions further in the next section. For large transverse momenta $p_T \gg Q_s$, however, the equations of motion can be linearized and one can express the classical gauge fields produced in the nuclear collision as [5, 35, 36, 37]

$$p^2 A^{\mu, a}(\mathbf{p}) = -i f_{abc} g^3 \int \frac{d^2 \mathbf{k}_T}{(2\pi)^2} L^\mu(\mathbf{p}, \mathbf{k}_T) \frac{\rho_1^b(\mathbf{k}_T) \rho_2^c(\mathbf{p}_T - \mathbf{k}_T)}{\mathbf{k}_T^2 (\mathbf{p}_T - \mathbf{k}_T)^2}. \quad (2.3)$$

Here f_{abc} are the SU(3) structure constants, L^μ is the well known⁴ Lipatov vertex and ρ_1, ρ_2 are respectively the Fourier transforms of the color charge densities in the two nuclei [3].

From eq. (1.1), the average in eq. (2.1) corresponds to

$$\langle \mathcal{O} \rangle \equiv \int [D\rho_1 D\rho_2] Z[\rho_1] Z[\rho_2] \mathcal{O}[\rho_1, \rho_2]. \quad (2.4)$$

In the MV model [1, 38]

$$Z[\rho] \equiv \exp \left(- \int d^2 \mathbf{x}_T \frac{\rho^a(\mathbf{x}_T) \rho^a(\mathbf{x}_T)}{2 \mu_A^2} \right), \quad (2.5)$$

where ρ can be either ρ_1 or ρ_2 . As we will discuss further in the next section, the color charge squared per unit area μ_A^2 can be expressed simply in terms of Q_s . We will consider this Gaussian model in the rest of this paper⁵. For these Gaussian correlations, in momentum space,

$$\left\langle \rho^a(\mathbf{k}_T) \rho^b(\mathbf{k}'_T) \right\rangle = (2\pi)^2 \mu_A^2 \delta^{ab} \delta(\mathbf{k}_T - \mathbf{k}'_T). \quad (2.6)$$

Using eq. (2.3), (2.4) and (2.5) in eq. (2.1), one obtains [22],

$$C(\mathbf{p}, \mathbf{q}) = \frac{S_\perp}{16 \pi^7} \frac{(g^2 \mu_A)^8}{g^4 Q_s^2} \frac{N_c^2 (N_c^2 - 1)}{p_T^4 q_T^4}. \quad (2.7)$$

It is instructive to express the result in eq. (2.7) in terms of the inclusive single gluon spectrum. This result, due originally to Gunion and Bertsch [40], has been recovered previously in the CGC framework [5, 35, 41, 42] and is known to have the form

$$\left\langle \frac{dN}{dy_p d^2 \mathbf{p}_T} \right\rangle = \frac{S_\perp}{4\pi^4} \frac{(g^2 \mu_A)^4}{g^2} \frac{N_c (N_c^2 - 1)}{p_T^4} \ln \left(\frac{p_T}{Q_s} \right). \quad (2.8)$$

Substituting eq. (2.8) on the r.h.s of eq. (2.7), one obtains

$$C(\mathbf{p}, \mathbf{q}) = \frac{\kappa_2}{S_\perp Q_s^2} \left\langle \frac{dN}{dy_p d^2 \mathbf{p}_T} \right\rangle \left\langle \frac{dN}{dy_q d^2 \mathbf{q}_T} \right\rangle, \quad (2.9)$$

which is the result we noted in eq. (1.4), with⁶

$$\kappa_2 \approx \frac{\pi}{(N_c^2 - 1)} = 0.4 \quad (2.10)$$

Identifying the theoretical error on κ_2 is difficult at this stage from the perturbative computation.

Computing κ_2 non-perturbatively by numerically solving the Yang-Mills equations is the primary objective of this paper. This quantity is not a pure number but can contain

⁴The components of this four vector are given explicitly by $L^+(\mathbf{p}, \mathbf{k}_T) = -\frac{\mathbf{k}_T^2}{p^-}$, $L^-(\mathbf{p}, \mathbf{k}_T) = \frac{(\mathbf{p}_T - \mathbf{k}_T)^2 - p_T^2}{p^+}$, $L^i(\mathbf{p}, \mathbf{k}_T) = -2 \mathbf{k}_T^i$.

⁵In the simplest treatment of small x evolution, based on the Balitsky-Kovchegov equation [11], $Z[\rho]$ can also be modelled by a Gaussian, albeit one with a non-local variance [37, 39].

⁶In the computation of Ref. [22], there were numerical errors which gave a significantly larger perturbative estimate for κ_2 .

interesting structure. In the perturbative calculation, κ_2 is independent of the relative angle $\Delta\varphi$ at very large transverse momenta $p_T, q_T \gg Q_s$. However, even in the perturbative calculations, one notices that there are finite azimuthal correlations between gluons as one goes away from the limit of asymptotically large transverse momenta. It is important to understand these correlations at momenta of interest to experiment to ascertain whether they have any phenomenological significance. Further, κ_2 can depend non-trivially on the transverse momenta of the pairs and on the energy and centrality of the nuclear collision. Finally, we want to determine whether κ_2 is infrared finite. This was the case for the analogous factor for the non-perturbative single gluon distribution at any finite time [14]; there is no guarantee that this should be the case for multi-gluon distributions.

Before we end this section, we should mention that perturbative computations were also performed for 3-gluon [32] and n -gluon correlations [33]. The result can be nicely summarized in terms of the cumulants of the multiplicity distribution as [33]

$$\left\langle \frac{d^n N}{dy_1 d^2\mathbf{p}_{T1} \cdots dy_n d^2\mathbf{p}_{Tn}} \right\rangle = \frac{(n-1)!}{k^{n-1}} \left\langle \frac{dN}{dy_1 d^2\mathbf{p}_{T1}} \right\rangle \times \cdots \times \left\langle \frac{dN}{dy_n d^2\mathbf{p}_{Tn}} \right\rangle, \quad (2.11)$$

where

$$k = \zeta \frac{(N_c^2 - 1)Q_s^2 S_\perp}{2\pi}. \quad (2.12)$$

Here ζ , is a non-perturbative coefficient⁷ to be determined by numerical solutions of Yang-Mills equations. The expression in eq. (2.11) corresponds to a negative binomial distribution. One can extract ζ from fits to the multiplicity distribution data [34] and compare our non-perturbative result for κ_2 to this value thereby testing the validity of eq. (2.11) for the 2nd cumulant. Our approach can be straightforwardly be extended to higher cumulants but the computations are numerically intensive and will not be considered further here.

3. Non-perturbative computation

The two gluon cumulant, on dimensional grounds, can always be expressed in the form given in eq. (2.9). However, as we have noted previously, the dimensionless coefficient κ_2 can in general be a function of $Q_s/p_T, Q_s/q_T, \Delta\varphi, Q_s R_A$ and m/Q_s , where m is an infrared regulator scale that can be added to the MV model. If we assume that $m \sim \Lambda_{\text{QCD}}$, the high energy asymptotics of our formalism is $m/Q_s \ll 1$ and $Q_s R_A \rightarrow \infty$. For A+A collisions at realistic RHIC and LHC energies, one expects $m/Q_s \sim 0.2 - 0.1$ and $Q_s R_A = 35 - 70$ respectively. We will return to the discussion of the infrared scale m later at the end of sec. 4.

For asymptotically large $p_T, q_T \gg Q_s$, we anticipate, on the basis of our perturbative results, that $\kappa_2 \rightarrow \text{constant}$. For $p_T, q_T \leq Q_s$, we will determine the dependence of κ_2 on these ratios. In particular, we would like to determine whether the double inclusive gluon distribution is rendered infrared safe by the non-linearities of the Yang-Mills fields that may generate a mass scale (analogous to a plasmon mass) for finite times $\tau \gtrsim 1/Q_s$.

⁷In the perturbative computation for the two and three particle correlations, this number was taken to be $\zeta = 2$.

3.1 Numerical approach

The numerical solutions of the classical Yang–Mills equations have been discussed at length elsewhere [14, 15, 17] and we will only outline the approach followed here for completeness. In the MV model [1], the Yang-Mills equations

$$[D_\mu, F^{\mu\nu}] = J^\nu. \quad (3.1)$$

have the source currents

$$J^\mu = \delta^{\mu+} \rho_1(\mathbf{x}_T, x^-) + \delta^{\mu-} \rho_2(\mathbf{x}_T, x^+), \quad (3.2)$$

where the color charge densities $\rho_{1,2}$ of the two nuclei are independent static color sources localized on the light cone $\rho_{1,2}(\mathbf{x}_T, x^\mp) \sim \rho_{1,2}(\mathbf{x}_T) \delta(x^\mp)$. They are distributed with the Gaussian probability distribution

$$\langle \rho^a(\mathbf{x}_T) \rho^b(\mathbf{y}_T) \rangle = g^2 \mu_A^2 \delta^{ab} \delta^2(\mathbf{x}_T - \mathbf{y}_T), \quad (3.3)$$

where \mathbf{x}_T and \mathbf{y}_T are vectors in the transverse plane. The initial conditions for the solutions of these equations in the forward light cone in the Fock–Schwinger gauge ($A^\tau = 0$) are given by

$$\begin{aligned} A^i|_{\tau=0} &= A_1^i + A_2^i, \\ A^\eta|_{\tau=0} &= \frac{ig}{2} [A_1^i, A_2^i], \end{aligned} \quad (3.4)$$

with

$$A_{1,2}^i = -\frac{i}{g} V_{1,2} \partial^i V_{1,2}^\dagger \quad \text{and} \quad \nabla_T^2 \Lambda_{1,2} = -g \rho_{1,2}. \quad (3.5)$$

where

$$V_{1,2} = \mathcal{P}_\mp e^{i\Lambda_{1,2}}. \quad (3.6)$$

It is convenient in the forward light cone to use the co-ordinate system $(\tau, \eta, \mathbf{x}_T)$, where $\tau^2 = t^2 - z^2$ and $\eta = 0.5 \ln((t+z)/(t-z))$. The Yang-Mills equations in this co-ordinate system are manifestly boost invariant with the gauge fields independent of η , namely, $A^\mu \equiv A^\mu(\tau, \mathbf{x}_T)$. The symbol \mathcal{P}_\mp denotes path ordering in the \mp directions of the Wilson line $V_{1,2}$ respectively, which for nucleus 1 (nucleus 2) have an implicit dependence on x^- (x^+) in the solution. We will return to this point at the end of the subsection.

A subtle point we would like to emphasize is that the Wilson lines V , in the gauge field solution given by eq. (3.5) for nucleus 1 (nucleus 2) before the collision, are path ordered in x^- (x^+). This feature of the continuum solution is implemented by constructing the Wilson lines in consecutive steps representing a discretization of the longitudinal coordinate. On each lattice site \mathbf{x}_T one constructs random color charges with a local Gaussian distribution

$$\langle \rho_k^a(\mathbf{x}_T) \rho_l^b(\mathbf{y}_T) \rangle = \delta^{ab} \delta^{kl} \delta^2(\mathbf{x}_T - \mathbf{y}_T) \frac{g^2 \mu_A^2}{N_y}, \quad (3.7)$$

with the indices $k, l = 1, \dots, N_y$ representing a discretized longitudinal coordinate. Numerical calculations of the single inclusive gluon distributions previously used $N_y = 1$,

whereas the derivation of the analytical expression in eq. (3.5) required an extended source corresponding to the limit $N_y \rightarrow \infty$.

Our normalization is chosen to give

$$\sum_{k,l} \left\langle \rho_k^a(\mathbf{x}_T) \rho_l^b(\mathbf{y}_T) \right\rangle = \delta^{ab} \delta^2(\mathbf{x}_T - \mathbf{y}_T) g^2 \mu_A^2. \quad (3.8)$$

The Wilson lines for the initial condition are then constructed from the sources eq. (3.7) by solving a Poisson equation and exponentiating it to give

$$V_{1,2}(\mathbf{x}_T) = \prod_{k=1}^{N_y} \exp \left\{ -ig \frac{\rho_k^{1,2}(\mathbf{x}_T)}{\nabla_T^2 + m^2} \right\}. \quad (3.9)$$

Here we have introduced an additional infrared regulator m into the MV model; some kind of infrared cutoff is required for inverting the Laplace operator. The single inclusive gluon distribution, integrated over transverse momenta, turns out to be weakly dependent on the infrared cutoff. One of the central aims of this paper is to study whether this is also the case for correlations. The parameter m plays an important role in the interpretation of our results and we will return to it in our discussion of the results of our computations. We will return to the physical interpretation of the role of the parameter m later in our discussion. For large N_y the charge densities ρ_k in eq. (3.7) become small, and the individual elements in the product (3.9) approach identity. This is precisely the procedure that leads in the $N_y \rightarrow \infty$ limit to the continuum path ordered exponential in eq. (3.6).

The previous numerical computations of the single inclusive spectrum defined the gluon multiplicity in a manner that slightly deviates from the definition based on the LSZ formalism in eq. (1.2). In [17], taking advantage of the equipartition of energy in the classical theory, only the electric field parts of the numerical solution were used. Assuming a free dispersion relation the gluon multiplicity was taken to be

$$\frac{dN}{d^2\mathbf{k}_T dy} = \frac{1}{(2\pi)^2} \frac{2}{|\mathbf{k}_T|} \text{Tr} \left[\frac{1}{\tau} E^i(\mathbf{k}_T) E^i(-\mathbf{k}_T) + \tau E^\eta(\mathbf{k}_T) E^\eta(-\mathbf{k}_T) \right], \quad (3.10)$$

where the electric fields $E^i = \tau \dot{A}_i$ and $E^\eta = \dot{A}_\eta / \tau$ are time derivatives of the gauge potentials, defined here with the explicit factors of τ coming from the formulation of the theory in τ, η -coordinates. In Refs. [14, 15] the numerically obtained E - and A -fields were used to determine the dispersion relation of the interacting theory. This was then in turn used to determine the multiplicity, unlike the free dispersion relation assumed in eq. (1.2). In this work we use a definition that corresponds to eq. (1.2) and take the gluon spectrum as

$$\frac{dN}{d^2\mathbf{k}_T dy} = \frac{1}{(2\pi)^2} \text{Tr} \left\{ \frac{1}{\tau |\mathbf{k}_T|} E^i(\mathbf{k}_T) E^i(-\mathbf{k}_T) + \tau |\mathbf{k}_T| A_i(\mathbf{k}_T) A_i(-\mathbf{k}_T) \right. \quad (3.11)$$

$$\left. + \frac{1}{|\mathbf{k}_T|} \tau E^\eta(\mathbf{k}_T) E^\eta(-\mathbf{k}_T) + \frac{|\mathbf{k}_T|}{\tau} A_\eta(\mathbf{k}_T) A_\eta(-\mathbf{k}_T) \right. \quad (3.12)$$

$$\left. + i \left[E^i(\mathbf{k}_T) A_i(-\mathbf{k}_T) - A_i(\mathbf{k}_T) E^i(-\mathbf{k}_T) \right] \right\} \quad (3.13)$$

$$\left. + i \left[E^\eta(\mathbf{k}_T) A_\eta(-\mathbf{k}_T) - A_\eta(\mathbf{k}_T) E^\eta(-\mathbf{k}_T) \right] \right\}, \quad (3.14)$$

where the fields are evaluated in the 2-dimensional Coulomb gauge. The interference terms (3.13) and (3.14) are odd under the transformation $\mathbf{k}_T \rightarrow -\mathbf{k}_T$. They do not contribute when the gluon spectrum is averaged over the angle of \mathbf{k}_T , integrated over \mathbf{k}_T or averaged over configurations of the sources. Thus neglecting them was justified when one was interested in the single inclusive gluon spectrum. In the case of two-gluon correlations they cannot, however, be neglected⁸. Due to these interference terms, the symmetry $n(\mathbf{k}_T) = n(-\mathbf{k}_T)$ does not hold configuration by configuration, but only on the average. Thus the correlation function $C(\mathbf{p}_T, \mathbf{q}_T) \neq C(\mathbf{p}_T, -\mathbf{q}_T)$. In particular, there is a peak in the correlation at $\mathbf{p}_T = \mathbf{q}_T$, which without the interference terms (3.13) and (3.14) would, by symmetry, imply a similar peak at $\mathbf{p}_T = -\mathbf{q}_T$. The main numerical effect of including these terms is that the backward peak at $\mathbf{p}_T = -\mathbf{q}_T$ is significantly depleted.

3.2 Parameters in the computation

From the discussion in the previous subsection, the parameters in the numerical lattice computation are

- $g^2\mu_A$, the root mean square color charge density.
- N_y , the number of points in the discretization of the longitudinal (x^- or rapidity) direction.
- The infrared regulator m . When $m = 0$, the Poisson equation is solved by leaving out the zero transverse momentum mode. This procedure corresponds to an infrared cutoff given by the size of the system.
- The lattice spacing a .
- The number of transverse lattice sites N_T , giving the transverse size of the lattice $L = N_T a$.

Of the dimensionful parameters a , $g^2\mu_A$ and m , only the dimensionless combinations $g^2\mu_A a$ and ma appear in the numerical calculation. The continuum limit $a \rightarrow 0$ is taken by letting $N_T \rightarrow \infty$ such that $g^2\mu_A a \rightarrow 0$ and $g^2\mu_A L = g^2\mu_A a N_T$ is a constant. This constant is determined by the physics input of the calculation. We have $\pi R_A^2 = L^2$ and, as we shall discuss in the next subsection, $g^2\mu_A$ is simply related to the saturation scale Q_s . The physical combination $Q_s R_A$ relevant at RHIC and LHC energies will translate into corresponding values of $g^2\mu L$ in our computation. In sec. 4, we will explicitly translate our numerical results into physically relevant numbers. We note that there is another dimensionless combination $m/g^2\mu_A$ -we will study the sensitivity of our results to this ratio.

3.3 Relating $g^2\mu_A$ and Q_s on the lattice

The root mean squared color charge density $g^2\mu_A$ that appears in our Glasma computations can be simply related to the saturation scale Q_s extracted from deeply inelastic scattering experiments. In these experiments, the cross section for a virtual photon scattering off

⁸We thank F. Gelis for pointing this out to us.

a high energy hadron or nucleus is simply related to the dipole cross section of a quark-antiquark pair scattering off the hadron. This “dipole” cross-section is determined, in the CGC formalism, by the correlator of two Wilson lines in the fundamental representation of each of the nuclei before the collision as

$$\tilde{C}^F(\mathbf{x}_T - \mathbf{y}_T) = \langle \text{Tr} V^\dagger(\mathbf{x}_T) V(\mathbf{y}_T) \rangle, \quad (3.15)$$

with the expectation value $\langle \rangle$ evaluated with the distribution of the sources. For Gaussian correlators in the MV model of sources extended in the longitudinal direction,

$$\langle \rho^a(\mathbf{x}_T, x^-) \rho^b(\mathbf{y}_T, y^-) \rangle = g^2 \delta^{ab} \delta^2(\mathbf{x}_T - \mathbf{y}_T) \delta(x^- - y^-) \mu_A^2(x^-),$$

the Wilson line correlators can be computed analytically up to a logarithmic infrared cutoff that must be introduced in solving the Poisson equation in eq. (3.5). The result is

$$\tilde{C}^F(\mathbf{x}_T) \approx N_c \exp\left(\frac{C_F}{8\pi} \chi \mathbf{x}_T^2 \ln(m|\mathbf{x}_T|)\right), \quad (3.16)$$

with

$$\chi = g^4 \int dx^- \mu_A^2(x^-). \quad (3.17)$$

Alternately, the saturation scale \tilde{Q}_s , in the fundamental representation, is defined as the momentum corresponding to the maximum of $\mathbf{k}_T^2 \tilde{C}^F(\mathbf{k}_T)$, where $\tilde{C}^F(\mathbf{k}_T)$ is the Fourier transform of eq. (3.15). In this manner, one can relate the saturation scale to the root mean square color charge density.

The saturation scale defined previously is an inverse correlation length associated with the correlator of two Wilson lines in the fundamental representation. In a nuclear collision, it is the saturation scale in the adjoint representation that is relevant. It is defined, equivalently as the momentum corresponding to the maximum of $\mathbf{k}_T^2 \tilde{C}^A(\mathbf{k}_T)$, where $\tilde{C}^A(\mathbf{k}_T)$ is the Fourier transform of the correlator of two adjoint Wilson lines

$$C^A(\mathbf{x}_T) = \langle V_{ab}(\mathbf{x}_T) V_{ab}(0) \rangle, \quad (3.18)$$

with

$$V_{ab}(\mathbf{x}_T) = 2 \text{Tr} \left[t^a V^\dagger(\mathbf{x}_T) t^b V(\mathbf{x}_T) \right]. \quad (3.19)$$

With some algebra, in the large N_c limit, the adjoint representation correlator can be related to a higher correlator of fundamental representation Wilson lines

$$C^A(\mathbf{x}_T) = \left\langle \left| \text{Tr} \left[V^\dagger(\mathbf{x}_T) V(0) \right] \right|^2 - 1 \right\rangle. \quad (3.20)$$

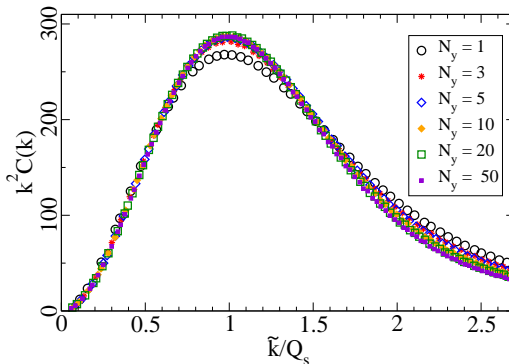


Figure 1: Adjoint representation Wilson line correlator for different N_y as a function of \mathbf{k}_T/Q_s . From Ref. [43].

In the Gaussian MV model, one obtains

$$C^A(\mathbf{x}_T) \approx (N_c^2 - 1) \exp\left(\frac{N_c}{8\pi} \chi \mathbf{x}_T^2 \ln(m|\mathbf{x}_T|)\right). \quad (3.21)$$

The saturation scale Q_s in the adjoint representation, in identical fashion to the fundamental case, is defined as the momentum corresponding to the maximum of $\mathbf{k}_T^2 \tilde{C}^A(\mathbf{k}_T)$, where $\tilde{C}^A(\mathbf{k}_T)$ is the Fourier transform of eq. (3.20). The adjoint Wilson line correlator is plotted in fig. 1 The two saturation scales are approximately related by the ratios of the Casimirs of the representations, namely, $Q_s^2 \approx \frac{C_A}{C_F} \tilde{Q}_s^2$.

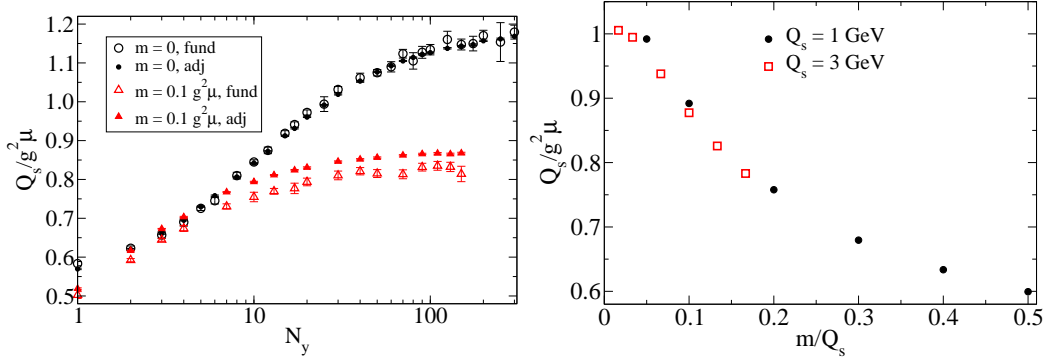


Figure 2: Left: $Q_s/g^2\mu_A$ versus N_y . From Ref. [43]. Right: Dependence of the ratio $Q_s/g^2\mu$ on m/Q_s for a fixed $Q_s = 1$ GeV and $N_y = 50$. These are the conversion factors used to obtain the m -dependence of our results for fixed Q_s in fig. 9.

Our definition of the saturation scale is not sensitive to the exact shape of the correlator for very large or small transverse momenta, and for a Gaussian correlator it reproduces the GBW saturation scale as $1/R_0^2 = \tilde{Q}_s^2$. For small momenta, the fundamental and adjoint correlators look like Gaussians, which is the form used in the “GBW” fit of DIS data in Refs. [44]. For large momenta there is a power law tail $1/\mathbf{k}_T^4$ that differs from the original GBW fits, but resembles more closely the form required to match smoothly to DGLAP evolution for large Q^2 [45].

In Ref. [43], the relation between Q_s and $g^2\mu_A$ was studied extensively employing numerical lattice techniques. Discretizing the longitudinal distribution of sources as described in eq. (3.7) and constructing the Wilson line as in eq. (3.9), it was shown that $Q_s \sim 0.57g^2\mu_A$ for $N_y = 1$. This value was used in the numerical Glasma simulations of the single inclusive gluon spectrum. As we shall see in the following the gluon spectrum, when expressed in terms of the scaling variable p_T/Q_s , is to a very good approximation independent of N_y . This is however not the case for the double inclusive spectrum, which will have a stronger dependence on N_y .

Due to the m -dependence of the single inclusive spectrum, the ratio κ_2 defined by eq. (1.4) will depend on m . To study this m -dependence for larger values of N_y (closer to the continuum limit in the longitudinal direction), we will need to invert the computation of Q_s as a function of $g^2\mu$ to obtain, as a function of m/Q_s , the required values of $g^2\mu$ corresponding to a fixed value of Q_s . The result of this exercise for $Q_s = 1$ GeV and 3 GeV and using the numerical method employed in [43] is shown in fig. 2.

4. Results

We begin the discussion of our numerical results with the single particle spectrum because we are interested in the ratio of the double inclusive spectrum to the single particle spectrum squared. Some of the results for the single particle spectrum are new and have not been published elsewhere. We will then proceed to discuss the double inclusive spectrum and state our results for κ_2 defined in eq. (1.4).

4.1 Single inclusive spectrum

The single inclusive multiplicity in A+A collisions was computed extensively previously by solving Yang-Mills equations numerically. We note that the single inclusive multiplicity computed gives excellent fits to the RHIC multiplicity data [16, 43] with values of Q_s for gold nuclei that agree to $\sim 10\%$ with those extracted from extrapolations of HERA data to RHIC [46]. In this sub-section, we will address some details of the computation that have not been presented previously and are relevant for the computation of κ_2 .

In Ref. [43], the dependence of the single inclusive gluon distribution as a function of N_y was not computed. We have done it here and the result is shown in fig. 3. It shows that the single inclusive spectrum, scaled in units of $(p_T/Q_s)^2$, shows virtually no N_y dependence in particular for the moderate p_T region that dominates the integrated multiplicity. We may conclude that it has a weak dependence on N_y (for fixed m/Q_s) addressing a concern raised in Ref. [47]. The numerical single particle spectrum in the UV region is sensitive to the lattice spacing a , which, for a fixed value of $Q_s R_A$, translates into a dependence on the size of the lattice N_T . As shown in fig. 3, the spectrum approaches the continuum ultraviolet behavior of Q_s^4/p_T^4 with increasing lattice sizes from $N_T = 128^2$ to $N_T = 512^2$ lattices.

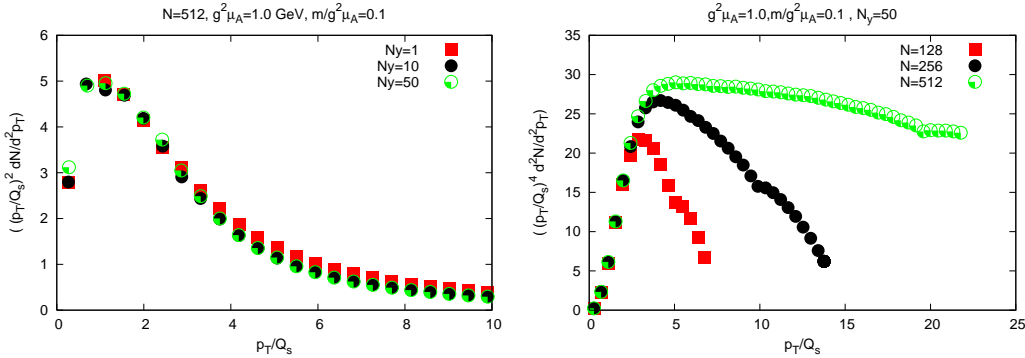


Figure 3: Left: The single particle spectrum (scaled by $(p_T/Q_s)^2$) for different N_y . Parameters are $g^2\mu = 1$ GeV, $N_T = 512$, IR cutoff fixed at $0.1g^2\mu$. Right: The single particle spectrum (scaled by $(p_T/Q_s)^4$) for different N_T . The continuum spectrum has a Q_s^4/p_T^4 behavior at $p_T \gg Q_s$; the convergence to this continuum behavior is clearly seen with increasing lattice size.

We studied the m/Q_s dependence of the single inclusive spectrum for a fixed large $N_y = 50$ and a 512×512 transverse lattice. The result is shown in fig. 4 (left). For small m/Q_s , the dependence of the spectrum on this quantity is quite weak-changing m/Q_s by a factor of 2

shows virtually no change in the spectrum. However, some dependence is seen when m/Q_s is increased, albeit the dependence is relatively weak in the $p_T \sim Q_s$ region which gives the dominant contribution to the integrated multiplicity. It should be kept in mind that the dependence of the spectrum on m/Q_s as shown is weaker than a logarithmic dependence even in the region where the dependence is the largest. It might seem counterintuitive that the value of an infrared scale m affects the gluon spectrum at such high momenta. One way to understand this is to keep in mind that the unitarity of the Wilson lines imposes a sum rule on their correlators, eqs. (3.15) and (3.20). Namely, because $\tilde{C}^F(\mathbf{x}_T - \mathbf{y}_T = 0) = N_c$, the integral of the momentum space correlator $\int d^2\mathbf{k}_T \tilde{C}^F(\mathbf{k}_T) = (2\pi)^2 N_c$ is a constant. Thus a modification of the distribution in the infrared will also affect the UV behavior, which is also reflected in the gluon spectrum.

Finally, we plot in fig. 4 (right) the dependence of the single particle spectrum on the other dimensionless combination of scales $g^2\mu L$ for fixed $m/g^2\mu$. (This corresponds to a very good approximation to fixed m/Q_s .) Virtually no dependence is seen on this quantity, confirming the expectation that the single inclusive spectrum is completely insensitive to physics on scales corresponding to the size of the system. In summary therefore, the single particle spectrum is most sensitive to physics at the scale Q_s , weakly sensitive to physics on the scale m and completely insensitive to physics on the scale $1/R$.

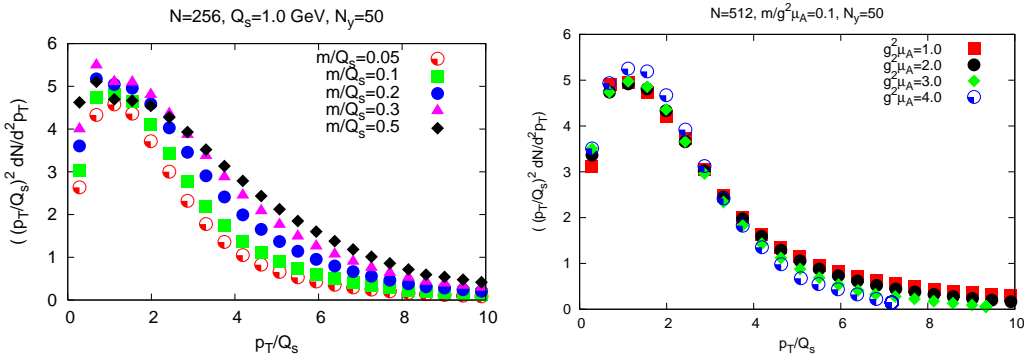


Figure 4: Left: The single particle spectrum for different m for $N_y = 50$, $N_T = 512$, and $Q_s = 1$ GeV. The spectrum is again scaled by $(p_T/Q_s)^2$. Right: The dependence of the single particle spectrum on $g^2\mu$ for a fixed $m/g^2\mu$.

4.2 Double inclusive spectrum

We now turn to the main focus of this study—the non-perturbative double inclusive gluon spectrum in A+A collisions. As in the single inclusive case studied in the previous section, we will first examine the sensitivity of the spectrum to the lattice parameters spelled out in section 3.2. Because the sensitivity of the single inclusive spectrum to these quantities is known to be weak, we will directly plot the dependence of κ_2 (see eq. (1.4)) on some of these quantities. After exploring the sensitivity of our results to lattice artifacts, we will quote results for the physical value of κ_2 , and discuss the implications of our results.

In fig. 5, we plot the correlated part of the double inclusive spectrum as a function of p_T/Q_s , the momentum of one of the tagged gluons, while holding the transverse momentum

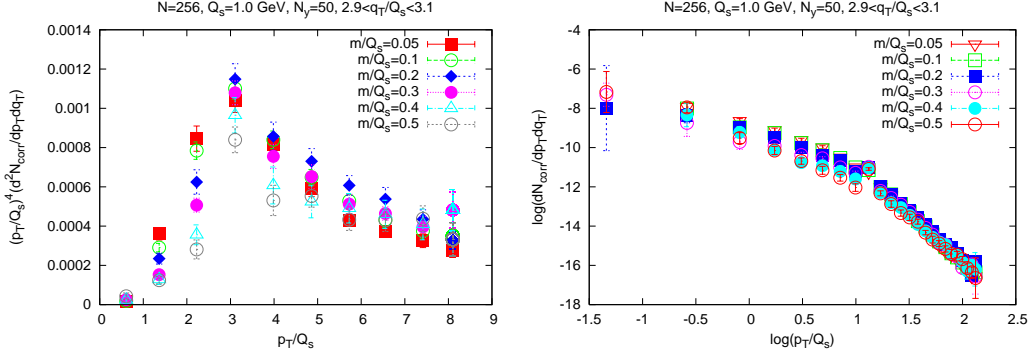


Figure 5: Sensitivity of the correlated part of the double inclusive spectrum to the value of IR cutoff m/Q_s . Left: Linear plot scaled by $(p_T/Q_s)^4$ to examine the anticipated perturbative behavior for large p_T . Right: Log-log plot of double correlated part of the double inclusive spectrum. The results are plotted for a small bin in q_T around $3Q_s$.

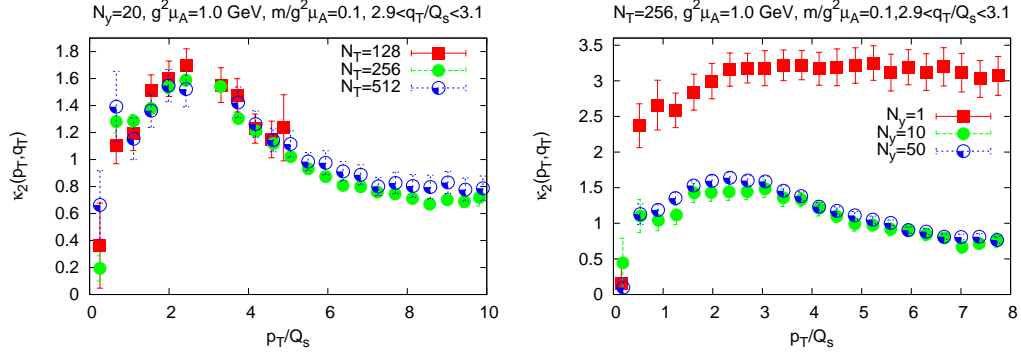


Figure 6: Left: Dependence of κ_2 on the transverse lattice size N_T as a function of p_T/Q_s for fixed q_T/Q_s . Right: Dependence of κ_2 on the number of points used in the construction of the path ordered exponential, N_y , as a function of p_T/Q_s for fixed q_T/Q_s .

q_T/Q_s of the other gluon fixed. The spectrum shown, plotted for different values of $m/g^2\mu$, is scaled by a factor $(p_T/Q_s)^4$ in fig. 5 (left). From the perturbative computation discussed in section 2, we expect this scaled spectrum to go to a constant value at large p_T/Q_s . We note that it does so approximately, keeping in mind that the spectrum at large p_T/Q_s is especially sensitive to lattice artifacts. We also note that the spectrum is weakly dependent on $m/g^2\mu$. In fig. 5 (right), we also plot the correlated double inclusive gluon spectrum as a log-log plot. In addition to the power law tail, we observe a qualitative change to a softer p_T spectrum for $p_T \leq 3Q_s$.

4.3 Determining κ_2

In fig. 6, we study the dependence of κ_2 on the number of transverse $N_T \times N_T$ lattice sites and on N_y , the number of points in the longitudinal direction used to construct the path ordered Wilson lines. In the former case, hardly any dependence is seen thereby indicating a rapid convergence to the continuum limit. For longitudinal lattices, one observes a strong dependence for small N_y , but a rapid convergence thereafter, with virtually no N_y

dependence seen for $N_y \geq 10$ onwards. The dependence of κ_2 on $g^2\mu L$ for a fixed value of $m/g^2\mu$ is shown in fig. 7. As anticipated, the dependence of κ_2 on $g^2\mu L$ is rather weak. This further confirms, as suggested previously, that the physics in the infrared is, for a finite m , insensitive to the size of the system R_A .

Now that we have established the convergence of κ_2 as a function of N_y and N_T is robust, we should remind the reader that the continuum value of κ_2 , being dimensionless, is most generally expressed as $\kappa_2(p_T/Q_s, q_T/Q_s, \Delta\varphi, Q_s R_A, m/Q_s)$. In general κ_2 is a function of two 2-dimensional vectors. When one takes into account rotational symmetry, it is a function of three variables and there are many ways to plot such a function. The general structure is illustrated in fig. 8, where we show κ_2 as a function of $|\mathbf{p}_T - \mathbf{q}_T|$ and $|\mathbf{p}_T + \mathbf{q}_T|$. There is a delta-function peak at $\mathbf{p}_T = \mathbf{q}_T$ which is clearly visible. The peak is left out in the right hand plot of fig. 8 to better illustrate the remaining structure. As mentioned in sec. 3.1, there is also an enhancement in the correlation in the back-to-back configuration $\mathbf{p}_T = -\mathbf{q}_T$, which can be clearly seen in fig. 8.

We now address the dependence of κ_2 on m/Q_s . We saw in fig. 5 that the double inclusive spectrum had a weak dependence on $m/g^2\mu$, but the single inclusive spectrum had a slightly stronger dependence. The resulting effect on κ_2 is shown in fig. 9 as a function of p_T with q_T averaged over the interval $[2.9 Q_s, 3.1 Q_s]$ and as a function of the angle between \mathbf{p}_T and \mathbf{q}_T . One observes that κ_2 decreases rapidly with increasing m/Q_s but converges to $\kappa_2 \sim 0.5$ for larger m/Q_s . The interpretation of the m/Q_s dependence of the results will be discussed further in the next section.

We can establish from the r.h.s. plot in fig. 9 that κ_2 is nearly constant as a function of $\Delta\varphi$; the strength of the correlation is only weakly dependent on the relative azimuthal angle between pairs of gluons. This result confirms the conjecture in Ref. [22]. Turning to the dependence of κ_2 on $p_T/Q_s, q_T/Q_s$, the dependence is not entirely flat as assumed in Ref. [22]; nevertheless, despite some structure, the variation of κ_2 with p_T/Q_s is on the order of 20% for $p_T/Q_s \leq 4$.

Figures 10 and 11 show the effect of taking different configurations of the “trigger” and “associate” transverse momenta p_T and q_T . In fig. 10 (left) the momentum q_T is fixed to three different narrow bins and κ_2 is plotted as a function of p_T . Figure 10 (right) shows the dependence of κ_2 on the angle between \mathbf{p}_T and \mathbf{q}_T for three different combinations of p_T and q_T ; either both around Q_s , both around $3Q_s$ or one at Q_s and the other one at $3Q_s$. In fig. 11, we show κ_2 for p_T and q_T having the same value, but with a finite angle between the vectors \mathbf{p}_T and \mathbf{q}_T ; showing a strong increase in the correlation for smaller values of the momenta.

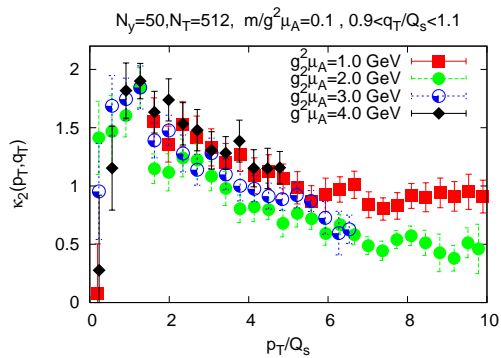


Figure 7: κ_2 for differing values of $g^2\mu L$ for a fixed $m/g^2\mu$ which is equivalent here to a fixed m/Q_s .

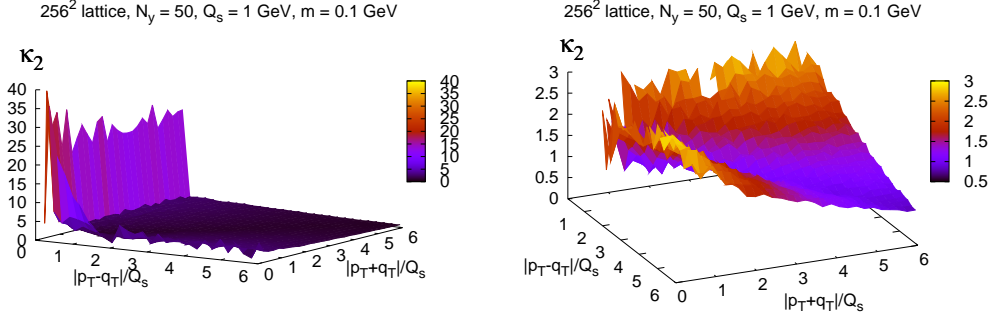


Figure 8: Three dimensional plot of $\kappa(|\mathbf{p}_T - \mathbf{q}_T|, |\mathbf{p}_T + \mathbf{q}_T|)$. The plot on the left shows the delta function peak at $\mathbf{p}_T = \mathbf{q}_T$. On the plot on the right this peak has been left out by reducing the range (the $|\mathbf{p}_T - \mathbf{q}_T|/Q_s$ -axis starts from 0.1) to show the structure around the away-side, i.e. close to $\mathbf{p}_T = -\mathbf{q}_T$.

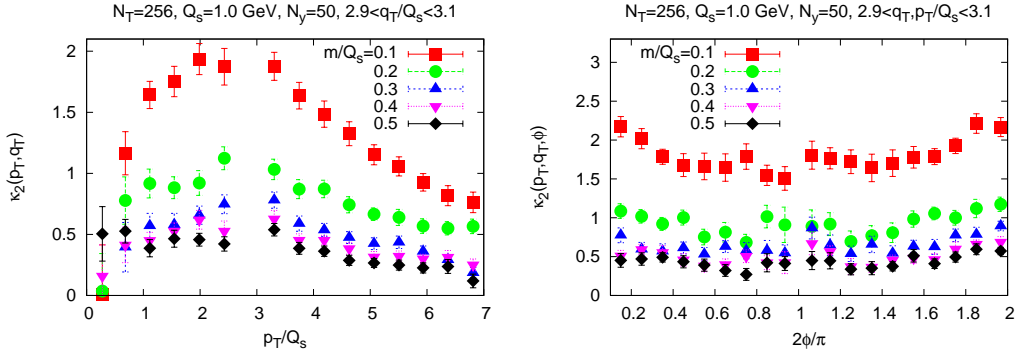


Figure 9: κ_2 for different values of m/Q_s with $Q_s = 1$ GeV, at $N_y = 50$. Left: κ_2 as a function of p_T for q_T in a small bin around $3Q_s$. Right: κ_2 as a function of $\Delta\phi$ with both p_T and q_T in a small bin around $3Q_s$.

5. Discussion and physical interpretation of results

We shall now discuss the physical implications of our numerical results for the double inclusive gluon distribution in the Glasma. In the Glasma flux tube picture [22], as noted in eq. (1.4) previously, it was conjectured that the correlated two gluon spectrum $C(\mathbf{p}, \mathbf{q})$ can be expressed as

$$\frac{C_2(\mathbf{p}, \mathbf{q})}{\left\langle \frac{dN}{dy_p d^2\mathbf{p}_T} \right\rangle \left\langle \frac{dN}{dy_q d^2\mathbf{q}_T} \right\rangle} = \kappa_2 \frac{1}{S_\perp Q_s^2}, \quad (5.1)$$

where κ_2 is a non-perturbative constant which behaves parametrically as N_c^{-2} . The perturbative computation of κ_2 has a logarithmic dependence on p_T/Q_s and q_T/Q_s . Modulo

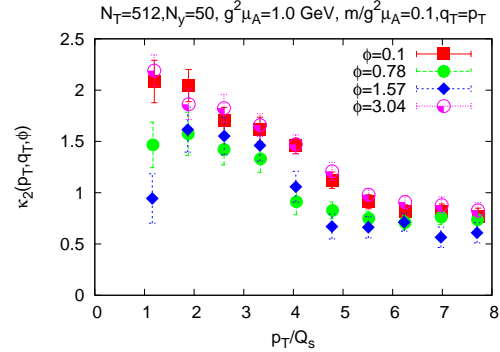


Figure 11: κ as function of momentum at equal momenta and specified angular separation.

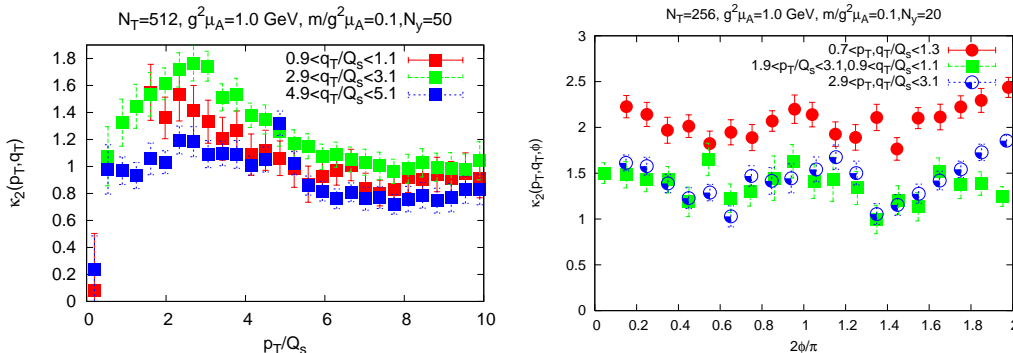


Figure 10: Left: κ as a function of absolute value of one of the momenta, the other being fixed to the specified value. Right: Angular dependence of κ at different absolute values of the momenta. Note absence of δ -function (point at $\Delta\varphi = 0$ outside plotted range on the y -axis) at unequal momenta.

this logarithm, one estimates perturbatively⁹ that $\kappa_2 \sim 0.4$.

In comparing our non-perturbative results to the perturbative estimate, we first note that κ_2 is weakly dependent on $\Delta\varphi$ and p_T/Q_s , q_T/Q_s , just as conjectured in Ref. [22]. Our result for κ_2 is larger than the perturbative estimate, but it has a sensitivity, as shown in fig. 9, to m/Q_s . As noted previously, the double inclusive spectrum by itself has a relatively weak dependence on m/Q_s and the dependence on m/Q_s in the ratio κ_2 mostly comes from the single inclusive spectrum. Let us now discuss the physical interpretation of this dependence.

Recall that in our computation m appeared as a cutoff inserted into eq. (3.9) to invert the Laplace operator. It regulates the long distance Coulomb tails of the color field¹⁰. In the context of the MV model, this scale appears as an additional external parameter, whose value is not determined within the model itself. Thus it is not completely clear whether the scale m should be thought of as the confinement scale or a scale of order Q_s . In a straightforward implementation it is natural to think of m as a cutoff imposing color neutrality at the size of a nucleon. This is indeed the picture used for instance in Refs. [18].

This picture does not, however, take into account color screening effects coming from quantum evolution effects (virtual and radiative corrections) that are described by the JIMWLK and BK equations. At RHIC energies they may not be very important but will be extremely important at LHC energies. The effect of color screening of the correlators has been considered previously [48] (see also the discussion in Ref. [33]) and it is argued that quantum evolution effects regulate the infrared behavior of the color charge density correlator at a scale that is also parametrically of the order of Q_s . This is not a purely classical effect arising from non-linear Yang-Mills dynamics but from a combination of rescattering and quantum evolution effects. To determine the “correct” value of m in this context it is thus necessary to go beyond the MV model and include the effects of high

⁹On account of incorrect factors of 2 and π , the number quoted in Ref. [22] is an order of magnitude larger. The correct perturbative value (modulo logs) is quoted in Refs. [33, 32].

¹⁰The propagator for the 2 dimensional Laplace operator is a logarithm.

energy evolution. A systematic numerical study of the two gluon correlation when high energy evolution effects are included is beyond the scope of this work.

A practical way to address this question in our simulation is to note that for a geometrical flux tube picture to be valid the two particle cumulant should be given by the size of the flux tube S_{ft} (representing the transverse range of color correlations) divided by the transverse area of the system times a number of order unity. We can make this logic explicit by expressing the size of the typical flux tube as

$$\frac{C_2(\mathbf{p}, \mathbf{q})}{\left\langle \frac{dN}{dy_p d^2\mathbf{p}_T} \right\rangle \left\langle \frac{dN}{dy_q d^2\mathbf{q}_T} \right\rangle} = \frac{S_{\text{ft}}}{S_{\perp}}, \quad (5.2)$$

where $S_{\text{ft}} = \kappa_2(\dots, m/Q_s)/Q_s^2$. For the range of $m/Q_s = 0.1-0.5$ considered, $\kappa_2 \approx 2 - 0.5$ converging rapidly to the latter value for increasing m/Q_s . The effective scale governing correlation strengths of unit strength is then $1/\sqrt{S_{\text{ft}}} \approx 0.7-1.4 Q_s$. This scale, although not numerically very large, is nevertheless a semi-hard scale and corresponds to transverse distances much smaller than the nucleon size, thereby confirming the picture of early times in the Glasma as classical field configurations that are coherent over transverse distances much smaller than a nucleon.

Let us then turn to a comparison with the RHIC data on two particle correlations. The experimentally observed quantity is $\Delta\rho/\sqrt{\rho_{\text{ref}}}(\Delta\varphi)$; in our framework, for $\Delta\varphi = 0$, it can be expressed as

$$\begin{aligned} \frac{\Delta\rho}{\sqrt{\rho_{\text{ref}}}}(\Delta\varphi = 0) &= \frac{dN}{dy} \cdot \frac{C_2(\mathbf{p}, \mathbf{q})}{\left\langle \frac{dN}{dy_p d^2\mathbf{p}_T} \right\rangle \left\langle \frac{dN}{dy_q d^2\mathbf{q}_T} \right\rangle} \left(\gamma_B - \frac{1}{\gamma_B} \right) \\ &= \frac{K_N}{\alpha_s} \left(\gamma_B - \frac{1}{\gamma_B} \right), \end{aligned} \quad (5.3)$$

where $K_N = \kappa_2/13.5$ for an SU(3) gauge theory and γ_B is the average radial boost in the framework of a blast wave model. From the RHIC data [28, 29], one can estimate that $\Delta\rho/\sqrt{\rho_{\text{ref}}}(\Delta\varphi = 0) = 1/\sqrt{2\pi\sigma_\varphi^2}$, with $\sigma_\varphi = 0.64$. Combining this with eq. (5.3), one obtains

$$\kappa_2^{\text{BW}} \sim \frac{0.7}{\left(\gamma_B - \frac{1}{\gamma_B} \right)}, \quad (5.4)$$

for $\alpha_s = 0.5$ and where the superscript denotes that this is a crude estimate extracted from experiment using a blast-wave parametrization. For an average blast wave radial velocity $V_r = 0.6$, this gives $\kappa_2^{\text{BW}} \sim 1.5$; for $V_r = 0.7$, one obtains $\kappa_2^{\text{BW}} \sim 1$. There is considerable variation therefore in the value of κ_2^{BW} obtained from the ridge data due to the final state flow parametrization.

An alternative method to extract κ_2 is to compare the expression for the *negative binomial* multiplicity distribution (cf. eqs. (2.11)–(2.12) in the Glasma [33] to PHENIX data [34] on the same. From this comparison, one obtains

$$\kappa_2^{\text{NBD}} \sim 3.9. \quad (5.5)$$

One sees therefore considerable variation in the extraction of κ_2 from experiment within the present framework. Within the many uncertainties, one can say at best it is a number

of order unity. Our study suggests that a coherent picture of such correlations from RHIC and higher LHC energies can in principle provide unique information on color screening of strong fields at early times in heavy ion collisions.

An objective of this study is also to proceed in the opposite direction, namely, to determine κ_2 from a non-perturbative computation and use this as input into a dynamical space-time evolution model. As guide to this future program is the work in Ref. [49], where two particle correlations are extracted from the hydrodynamical evolution of flux tube structures in A+A collisions.

6. Summary

In this paper, we investigated the validity of the Glasma flux tube scenario of multi-particle correlations by performing a non-perturbative numerical computation of double inclusive gluon production in the Glasma. Our results were obtained by solving Yang-Mills equations on a space-time lattice for Gaussian distributed color source configurations with a variance proportional to the saturation scale Q_s^2 . Our results confirm key features of the Glasma flux tube scenario. Particles produced from coherent longitudinal electric and magnetic fields in transverse regions of size $\sim 1.4/Q_s - 1/2 Q_s$, much smaller than the nucleon size, have correlations of unit strength. As in the asymptotic perturbative estimates, particles produced from the flux tubes are uncorrelated in the relative azimuthal angle between the particles, the observed azimuthal collimation being produced later from radial flow. The correlations show non-trivial structure in p_T and q_T , which smoothly go over to perturbative results in the limit of $p_T/Q_s \gg 1$, $q_T/Q_s \gg 1$. Our results for the two particle correlation strength are consistent with estimates of the strength extracted from model comparisons to RHIC data. A useful extension of this work is to incorporate our results into more detailed hydrodynamical models of the space-time evolution of initial state correlations.

7. Acknowledgments

We thank Adrian Dumitru, Sean Gavin, Larry McLerran and Jun Takahashi for very helpful discussions. We are especially grateful to François Gelis for numerous useful remarks and insights that have significantly improved this work. S.S.'s research is supported by a SCIDAC grant and by a Lab Directed Research & Development (LDRD) grant from Brookhaven National Laboratory. R.V.'s research is supported by DOE Contract No. DE-AC02-98CH10886. T.L. is supported by the Academy of Finland, project 126604.

A. Lattice formulation

The Yang-Mills equations can be formulated as Hamilton's equations of motion. To preserve gauge invariance, they are solved numerically on a lattice where the degrees of freedom at a site i are the link variables

$$U_i(\mathbf{x}_T) = \exp[igaA_i(\mathbf{x}_T)], \quad (\text{A.1})$$

where a is the lattice spacing on a transverse lattice. The appropriate discretized lattice (Kogut-Susskind) Hamiltonian in our case is given by

$$aH = \sum_{\mathbf{x}_T} \left\{ \frac{g^2 a}{\tau} \text{Tr} E^i E^i + \frac{2N_c \tau}{g^2 a} \left(1 - \frac{1}{N_c} \text{Re} \text{Tr} U_{\square} \right) + \frac{\tau}{a} \text{Tr} \pi^2 + \frac{a}{\tau} \sum_i \text{Tr} \left(\phi - \tilde{\phi}_i \right)^2 \right\}, \quad (\text{A.2})$$

where E_i, U_i, π and ϕ are dimensionless lattice fields that are matrices in color space, with $E^i = E_a^i t_a$ etc. and the generators of the fundamental representation normalised as $\text{Tr} (t_a t_b) = \delta_{ab}/2$.

The first two terms are the transverse electric and magnetic fields with the transverse plaquette defined as

$$U_{\square}(\mathbf{x}_T) = U_x(\mathbf{x}_T) U_y(\mathbf{x}_T + e_x) U_x^{\dagger}(\mathbf{x}_T + e_y) U_y^{\dagger}(\mathbf{x}_T). \quad (\text{A.3})$$

The last two terms are the kinetic energy and covariant derivative of the rapidity component of the gauge field $\phi \equiv A_{\eta} = -\tau^2 A^{\eta}$. The latter becomes an adjoint representation scalar following the assumption of boost invariance. For the parallel transported scalar field, we use the notation

$$\tilde{\phi}_i(\mathbf{x}_T) \equiv U_i(\mathbf{x}_T) \phi(\mathbf{x}_T + e_i) U_i^{\dagger}(\mathbf{x}_T). \quad (\text{A.4})$$

In the Hamiltonian, eq. (A.2), there is a residual invariance under gauge transformations depending only on the transverse coordinates.

The Hamiltonian equations of motion are

$$\dot{U}_i = i \frac{g^2}{\tau} E^i U_i \quad (\text{no sum over } i), \quad (\text{A.5})$$

$$\dot{\phi} = \tau \pi, \quad (\text{A.6})$$

$$\dot{E}^x = \frac{i\tau}{2g^2} [U_{x,y} + U_{x,-y} - \text{h.c.}] - \text{trace} + \frac{i}{\tau} [\tilde{\phi}_x, \phi] \quad (\text{A.7})$$

$$\dot{E}^y = \frac{i\tau}{2g^2} [U_{y,x} + U_{y,-x} - \text{h.c.}] - \text{trace} + \frac{i}{\tau} [\tilde{\phi}_y, \phi],$$

$$\dot{\pi} = \frac{1}{\tau} \sum_i [\tilde{\phi}_i + \tilde{\phi}_{-i} - 2\phi]. \quad (\text{A.8})$$

Gauss's law, conserved by the equations of motion, is given by

$$\sum_i \left[U_i^{\dagger}(\mathbf{x}_T - e_i) E^i(\mathbf{x}_T - e_i) U_i(\mathbf{x}_T - e_i) - E^i(\mathbf{x}_T) \right] - i[\phi, \pi] = 0.$$

On the lattice the initial conditions (3.4) are

$$0 = \text{Tr} \left[t_a \left((U_i^1 + U_i^2) \left(1 + U_i^{\dagger} \right) - \text{h.c.} \right) \right], \quad (\text{A.9})$$

$$E^i = 0, \quad (\text{A.10})$$

$$\phi = 0, \quad (\text{A.11})$$

$$\pi(\mathbf{x}_T) = \frac{-i}{4g} \sum_i \left[(U_i(\mathbf{x}_T) - 1) \left(U_i^{\dagger 2}(\mathbf{x}_T) - U_i^{\dagger 1}(\mathbf{x}_T) \right) \right. \quad (\text{A.12})$$

$$\left. + \left(U_i^{\dagger}(\mathbf{x}_T - e_i) - 1 \right) \left(U_i^2(\mathbf{x}_T - e_i) - U_i^1(\mathbf{x}_T - e_i) \right) - \text{h.c.} \right],$$

where $U_i^{1,2}$ in eq. (A.9) are the link matrices corresponding to the color fields of the two nuclei ($A_i^{1,2}$ in eq. (3.5)). The link matrix U_i , which corresponding to the $\tau \geq 0$ color field A_i , is determined by solving eq. (A.9).

References

- [1] L. D. McLerran and R. Venugopalan, *Phys. Rev.* **D49** (1994) 2233 [arXiv:hep-ph/9309289];
L. D. McLerran and R. Venugopalan, *Phys. Rev.* **D49** (1994) 3352 [arXiv:hep-ph/9311205];
L. D. McLerran and R. Venugopalan, *Phys. Rev.* **D50** (1994) 2225 [arXiv:hep-ph/9402335].
- [2] J. Jalilian-Marian, A. Kovner, L. D. McLerran and H. Weigert, *Phys. Rev.* **D55** (1997) 5414 [arXiv:hep-ph/9606337]; J. Jalilian-Marian, A. Kovner, A. Leonidov and H. Weigert, *Nucl. Phys.* **B504** (1997) 415 [arXiv:hep-ph/9701284]; J. Jalilian-Marian, A. Kovner, A. Leonidov and H. Weigert, *Phys. Rev.* **D59** (1999) 014014 [arXiv:hep-ph/9706377];
J. Jalilian-Marian, A. Kovner and H. Weigert, *Phys. Rev.* **D59** (1999) 014015 [arXiv:hep-ph/9709432]; J. Jalilian-Marian, A. Kovner, A. Leonidov and H. Weigert, *Phys. Rev.* **D59** (1999) 034007 [arXiv:hep-ph/9807462]; H. Weigert, *Nucl. Phys.* **A703** (2002) 823 [arXiv:hep-ph/0004044]; E. Iancu, A. Leonidov and L. D. McLerran, *Nucl. Phys.* **A692** (2001) 583 [arXiv:hep-ph/0011241]; E. Iancu and L. D. McLerran, *Phys. Lett.* **B510** (2001) 145 [arXiv:hep-ph/0103032]; E. Ferreiro, E. Iancu, A. Leonidov and L. McLerran, *Nucl. Phys.* **A703** (2002) 489 [arXiv:hep-ph/0109115]; E. Iancu, A. Leonidov and L. D. McLerran, *Phys. Lett.* **B510** (2001) 133 [arXiv:hep-ph/0102009]; A. H. Mueller, *Phys. Lett.* **B523** (2001) 243 [arXiv:hep-ph/0110169].
- [3] E. Iancu and R. Venugopalan in *Quark gluon plasma* (R. Hwa and X. N. Wang, eds.). World Scientific, 2003. arXiv:hep-ph/0303204; H. Weigert, *Prog. Part. Nucl. Phys.* **55** (2005) 461 [arXiv:hep-ph/0501087].
- [4] F. Gelis and R. Venugopalan, *Nucl. Phys.* **A776** (2006) 135 [arXiv:hep-ph/0601209];
F. Gelis and R. Venugopalan, *Nucl. Phys.* **A779** (2006) 177 [arXiv:hep-ph/0605246].
- [5] A. Kovner, L. D. McLerran and H. Weigert, *Phys. Rev.* **D52** (1995) 3809 [arXiv:hep-ph/9505320].
- [6] D. Kharzeev, A. Krasnitz and R. Venugopalan, *Phys. Lett.* **B545** (2002) 298 [arXiv:hep-ph/0109253].
- [7] T. Lappi and L. McLerran, *Nucl. Phys.* **A772** (2006) 200 [arXiv:hep-ph/0602189].
- [8] F. Gelis and R. Venugopalan, *Acta Phys. Polon.* **B37** (2006) 3253 [arXiv:hep-ph/0611157];
F. Gelis, T. Lappi and R. Venugopalan, *Int. J. Mod. Phys.* **E16** (2007) 2595 [arXiv:0708.0047 [hep-ph]].
- [9] F. Gelis, T. Lappi and R. Venugopalan, *Phys. Rev.* **D78** (2008) 054019 [arXiv:0804.2630 [hep-ph]].
- [10] F. Gelis, T. Lappi and R. Venugopalan, *Phys. Rev.* **D78** (2008) 054020 [arXiv:0807.1306 [hep-ph]].
- [11] I. Balitsky, *Nucl. Phys.* **B463** (1996) 99 [arXiv:hep-ph/9509348]; I. Balitsky, *Phys. Rev. Lett.* **81** (1998) 2024 [arXiv:hep-ph/9807434]; I. Balitsky, *Phys. Rev.* **D60** (1999) 014020 [arXiv:hep-ph/9812311]; Y. V. Kovchegov, *Phys. Rev.* **D60** (1999) 034008 [arXiv:hep-ph/9901281]; Y. V. Kovchegov, *Phys. Rev.* **D61** (2000) 074018 [arXiv:hep-ph/9905214]; I. Balitsky, *Phys. Lett.* **B518** (2001) 235 [arXiv:hep-ph/0105334].

- [12] J. P. Blaizot, F. Gelis and R. Venugopalan, *Nucl. Phys.* **A743** (2004) 57 [arXiv:hep-ph/0402257].
- [13] F. Gelis, T. Lappi and R. Venugopalan, *Phys. Rev.* **D79** (2008) 094017 [arXiv:0810.4829 [hep-ph]]; T. Lappi, *Acta Phys. Polon.* **B40** (2009) 1997 [arXiv:0904.1670 [hep-ph]].
- [14] A. Krasnitz and R. Venugopalan, *Nucl. Phys.* **B557** (1999) 237 [arXiv:hep-ph/9809433]; A. Krasnitz and R. Venugopalan, *Phys. Rev. Lett.* **84** (2000) 4309 [arXiv:hep-ph/9909203]; A. Krasnitz and R. Venugopalan, *Phys. Rev. Lett.* **86** (2001) 1717 [arXiv:hep-ph/0007108].
- [15] A. Krasnitz, Y. Nara and R. Venugopalan, *Phys. Rev. Lett.* **87** (2001) 192302 [arXiv:hep-ph/0108092].
- [16] A. Krasnitz, Y. Nara and R. Venugopalan, *Nucl. Phys.* **A727** (2003) 427 [arXiv:hep-ph/0305112].
- [17] T. Lappi, *Phys. Rev.* **C67** (2003) 054903 [arXiv:hep-ph/0303076]; T. Lappi, *Phys. Lett.* **B643** (2006) 11 [arXiv:hep-ph/0606207].
- [18] A. Krasnitz, Y. Nara and R. Venugopalan, *Phys. Lett.* **B554** (2003) 21 [arXiv:hep-ph/0204361]; A. Krasnitz, Y. Nara and R. Venugopalan, *Nucl. Phys.* **A717** (2003) 268 [arXiv:hep-ph/0209269]; T. Lappi and R. Venugopalan, *Phys. Rev.* **C74** (2006) 054905 [arXiv:nucl-th/0609021].
- [19] D. E. Kharzeev, L. D. McLerran and H. J. Warringa, *Nucl. Phys.* **A803** (2008) 227 [arXiv:0711.0950 [hep-ph]].
- [20] S. A. Voloshin, *Phys. Lett.* **B632** (2006) 490 [arXiv:nucl-th/0312065].
- [21] E. V. Shuryak, *Phys. Rev.* **C76** (2007) 047901 [arXiv:0706.3531 [nucl-th]].
- [22] A. Dumitru, F. Gelis, L. McLerran and R. Venugopalan, *Nucl. Phys.* **A810** (2008) 91 [arXiv:0804.3858 [hep-ph]].
- [23] S. Gavin, L. McLerran and G. Moschelli, *Phys. Rev.* **C79** (2009) 051902 [arXiv:0806.4718 [nucl-th]]; G. Moschelli and S. Gavin, arXiv:0910.3590 [nucl-th].
- [24] **STAR** collaboration, J. Adams *et. al.*, *Phys. Rev. Lett.* **95** (2005) 152301 [arXiv:nucl-ex/0501016].
- [25] **STAR** collaboration, F. Wang, *J. Phys.* **G30** (2004) S1299 [arXiv:nucl-ex/0404010]; **PHENIX** collaboration, A. Adare *et. al.*, *Phys. Rev.* **C78** (2008) 014901 [arXiv:0801.4545 [nucl-ex]]; **PHOBOS** collaboration, B. Alver *et. al.*, arXiv:0812.1172 [nucl-ex].
- [26] **STAR** collaboration, P. K. Netrakanti, *J. Phys.* **G35** (2008) 104010 [arXiv:0804.4417 [nucl-ex]]; **STAR** collaboration, B. I. Abelev *et. al.*, *Phys. Rev. Lett.* **102** (2009) 052302 [arXiv:0805.0622 [nucl-ex]].
- [27] **STAR** collaboration, L. Molnar, *J. Phys.* **G34** (2007) S593 [arXiv:nucl-ex/0701061]; **PHOBOS** collaboration, B. Alver *et. al.*, *J. Phys.* **G35** (2008) 104080 [arXiv:0804.3038 [nucl-ex]].
- [28] **STAR** collaboration, J. Adams *et. al.*, *Phys. Rev.* **C73** (2006) 064907 [arXiv:nucl-ex/0411003]; **STAR** collaboration, B. I. Abelev *et. al.*, *Phys. Rev.* **C80** (2009) 064912 [arXiv:0909.0191 [nucl-ex]].
- [29] **STAR** collaboration, M. Daugherty, *J. Phys.* **G35** (2008) 104090 [arXiv:0806.2121 [nucl-ex]].

- [30] N. Armesto, C. A. Salgado and U. A. Wiedemann, *Phys. Rev. Lett.* **93** (2004) 242301 [arXiv:hep-ph/0405301]; A. Majumder, B. Muller and S. A. Bass, *Phys. Rev. Lett.* **99** (2007) 042301 [arXiv:hep-ph/0611135]; V. S. Pantuev, arXiv:0710.1882 [hep-ph]; C.-Y. Wong, *Phys. Rev.* **C78** (2008) 064905 [arXiv:0806.2154 [hep-ph]]; C. B. Chiu and R. C. Hwa, *Phys. Rev.* **C79** (2009) 034901 [arXiv:0809.3018 [nucl-th]].
- [31] J. L. Nagle, *Nucl. Phys.* **A830** (2009) 147c [arXiv:0907.2707 [nucl-ex]].
- [32] K. Dusling, D. Fernandez-Fraile and R. Venugopalan, *Nucl. Phys.* **A828** (2009) 161 [arXiv:0902.4435 [nucl-th]].
- [33] F. Gelis, T. Lappi and L. McLerran, *Nucl. Phys.* **A828** (2009) 149 [arXiv:0905.3234 [hep-ph]].
- [34] **PHENIX** collaboration, A. Adare *et. al.*, *Phys. Rev.* **C78** (2008) 044902 [arXiv:0805.1521 [nucl-ex]].
- [35] A. Kovner, L. D. McLerran and H. Weigert, *Phys. Rev.* **D52** (1995) 6231 [arXiv:hep-ph/9502289].
- [36] A. Dumitru and L. D. McLerran, *Nucl. Phys.* **A700** (2002) 492 [arXiv:hep-ph/0105268].
- [37] J. P. Blaizot, F. Gelis and R. Venugopalan, *Nucl. Phys.* **A743** (2004) 13 [arXiv:hep-ph/0402256].
- [38] Y. V. Kovchegov, *Phys. Rev.* **D54** (1996) 5463 [arXiv:hep-ph/9605446].
- [39] H. Fujii, F. Gelis and R. Venugopalan, *Nucl. Phys.* **A780** (2006) 146 [arXiv:hep-ph/0603099].
- [40] J. F. Gunion and G. Bertsch, *Phys. Rev.* **D25** (1982) 746.
- [41] Y. V. Kovchegov and D. H. Rischke, *Phys. Rev.* **C56** (1997) 1084 [arXiv:hep-ph/9704201].
- [42] M. Gyulassy and L. D. McLerran, *Phys. Rev.* **C56** (1997) 2219 [arXiv:nucl-th/9704034].
- [43] T. Lappi, *Eur. Phys. J.* **C55** (2008) 285 [arXiv:0711.3039 [hep-ph]].
- [44] K. J. Golec-Biernat and M. Wusthoff, *Phys. Rev.* **D59** (1999) 014017 [arXiv:hep-ph/9807513]; K. J. Golec-Biernat and M. Wusthoff, *Phys. Rev.* **D60** (1999) 114023 [arXiv:hep-ph/9903358]; A. M. Stasto, K. J. Golec-Biernat and J. Kwiecinski, *Phys. Rev. Lett.* **86** (2001) 596 [arXiv:hep-ph/0007192].
- [45] J. Bartels, K. J. Golec-Biernat and H. Kowalski, *Phys. Rev.* **D66** (2002) 014001 [arXiv:hep-ph/0203258].
- [46] H. Kowalski, T. Lappi and R. Venugopalan, *Phys. Rev. Lett.* **100** (2008) 022303 [arXiv:0705.3047 [hep-ph]].
- [47] K. Fukushima, *Phys. Rev.* **D77** (2008) 074005 [arXiv:0711.2364 [hep-ph]].
- [48] E. Iancu, K. Itakura and L. McLerran, *Nucl. Phys.* **A724** (2003) 181 [arXiv:hep-ph/0212123]; A. H. Mueller, *Nucl. Phys.* **B643** (2002) 501 [arXiv:hep-ph/0206216].
- [49] J. Takahashi *et. al.*, *Phys. Rev. Lett.* **103** (2009) 242301 [arXiv:0902.4870 [nucl-th]].